THE JOURNAL OF PHYSICAL CHEMISTRY Letters

Letter

Cite This: J. Phys. Chem. Lett. 2019, 10, 4706−4712

pubs.acs.org/JPCL

Role of Halogen Atoms on High-Efficiency Mn^{2+} Emission in Two-Dimensional Hybrid Perovskites

Guojun Zhou,[†,#] Xiaofang Jia,[‡,#] Shaoqiang Guo,[‡] Maxim Molokeev,[⊥,∥,▽] Junying Zhang,*[,‡] and Zhiguo Xia*[,§,†]

[†]The Beijing Municipal Key Laboratory of New Energy Materials and Technologies School of Materials Sciences and Engineering, University of Science and Technology Beijing, Beijing 100083, China

[‡]Key Laboratory of Micro−Nano Measurement, Manipulation and Physics (Ministry of Education), School of Physics, Beihang University, Beijing 100191, China

[⊥]Laboratory of Crystal Physics, Kirensky Institute of Physics, Federal Research Center KSC SB RAS, Krasnoyarsk 660036, Russia

[∥]Siberian Federal University, Krasnoyarsk 660041, Russia

[▽]Department of Physics, Far Eastern State Transport University, Khabarovsk 680021, Russia

[§]State Key Laboratory of Luminescent Materials and Devices and Institute of Optical Communication Materials, South China University of Technology, Guangzhou 510641, China

Supporting Information

ABSTRACT: Doped halide pervoskites as highly efficient light emitters have recently fascinated the research community, while the influence of halogen atoms X (X = Cl, Br, I) on the hybrid energy levels and photoluminescence properties remains a challenge. Here, the role of X compositions in the two-dimensional hybrid perovskite BA_2PbX_4 (BA = $C_4H_9NH_3$) on the doped Mn^{2+} emission is identified, wherein Mn^{2+} reveals a strong luminescence dependence on the nature of the halogen, and optimum Mn^{2+} emission with a record quantum yield of 60.1% has been achieved in BA_2PbBr_4. Density functional theory calculations show that BA_2PbBr_4 holds low Br vacancy concentration and unique coupled states of the Mn-3d level and Pb-6p level at the conduction band minimum, leading to efficient energy transfer from the host to Mn^{2+}. Our work sheds new light on the methods to realize strong exciton−dopant exchange coupling for achieving high-efficiency dopant luminescence.

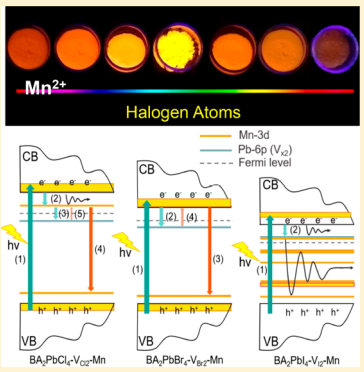

Hybrid metal halide pervoskites, as a family of emerging semiconductor optoelectronic materials, have received significant attention in recent years due to their impressive structural diversity and the emerging applications in the fields of solar cells, photodetectors, lasers, and light-emitting.[1−9] Doping of an impurity into metal halide pervoskites was found to be an effective approach to tuning the optoelectronic properties via the exciton−dopant exchange coupling, and the rational incorporation of impurity can favorably modulate the electronic and optical properties of the doped metal halides.[10,11] Until now, several examples of the amusing optical properties associated with these doped materials have been reported, and improvement of the performance can be realized.[12−15] The most commonly used impurity dopants to date are Mn^{2+}, Cu^{2+}, Cd^{2+}, and Bi^{3+},[11,16−23] and Mn^{2+} is one of the most attractive candidates, widely known for its long-lifetime Mn d−d orange emission. In recent years, Mn^{2+} ions have been doped not only in ABX_3 perovskite nanocrystals but also in double perovskites, two-dimensional (2D) pervoskites, and other low-dimensional metal halides.[10,16,19,24,25] It is noteworthy that Mn^{2+}-doped 2D layered pervoskites usually show enhanced energy transfer efficiency from the strongly bound excitons of the hosts to the d electrons of Mn^{2+} ions, resulting in intense emission due to the $^4T_1$ to $^6A_1$ transition.[10,16,26] However, it is undeniable that there are many factors affecting the luminescence efficiency of the doped ions, such as structure type, morphology, and ligand character.[12,13,16,17,27,28] Up to now, the influence of halogen types and contents on the luminescence of either the exciton or dopant has rarely been investigated in 2D hybrid pervoskites. To clarify this basic but very important issue, on the one hand, the correlation of the energy levels of Mn^{2+} ions, electronic structures of the BA_2PbX_4 (BA = $C_4H_9NH_3$) hosts, and the exciton−dopant exchange coupling effect and the energy transfer process involved has been carefully considered to realize the controlled emission. On the other hand, it is vital for the design and preparation of high-efficiency metal halides with dopant luminescence for solid-state lighting applications because the hybrid metal halide materials have attracted great attention due to their structural diversity and outstanding

Received: July 10, 2019
Accepted: July 30, 2019
Published: July 30, 2019

DOI: 10.1021/acs.jpclett.9b01996
J. Phys. Chem. Lett. 2019, 10, 4706−4712

optoelectronic properties, which make them promising candidates for light-emitting diodes (LEDs).

Herein, we introduce a family of Mn^{2+}-doped 2D hybrid pervoskites BA_2PbX_4 (X = Cl, Br, I) offering unique insights into the chemical mechanism of doping, as well as into the fundamental relationship between the halogen contents and the Mn^{2+} emission by density functional theory (DFT) calculations. Specifically, by elucidating the role of halogens on the X vacancy (V_{X1}, V_{X2}) defects and the electronic structure of host, we develop a general theory to optimize high-efficiency Mn^{2+} emission in 2D hybrid pervoskites. It clearly demonstrates that tuning of halogen contents is vital for optimizing luminescent properties of dopants. Our realizable cases could provide a new understanding of halogen atoms and propose a feasible approach to achieving high-efficiency dopant luminescence.

The target products were synthesized by a co-precipitation method with different raw material ratios, as illustrated in Figure S1a,b. The XRD patterns (Figure 1) indicate that all of

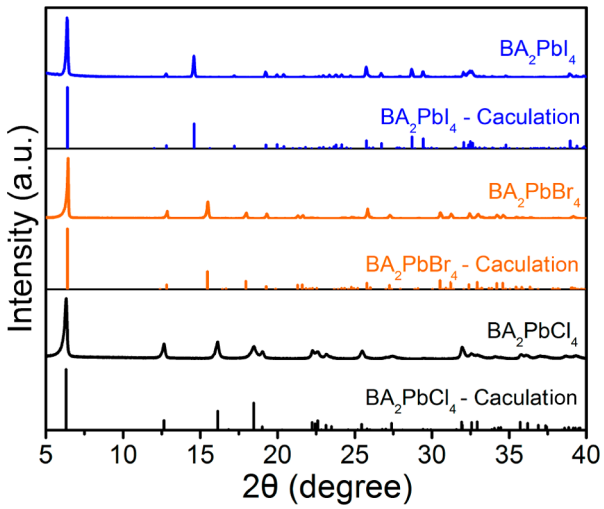

Figure 1. XRD patterns of the end-member compounds BA_2PbCl_4, BA_2PbBr_4, and BA_2PbI_4. The corresponding standard patterns obtained from the results of structural refinement can be used as references.

the BA_2PbX_4 (X = Cl, Br, I) compounds are pure-phase by comparison with the corresponding standard cards. According to the structural refinement analysis in Figure S2, the anisotropic model of the preferred orientation with second-order spherical harmonics was used due to the severely preferred orientation of microcrystals, and all peaks were indexed by an orthorhombic cell (*Pbca*). It is noteworthy that some amorphous glasses should be added to the samples to eliminate the preferred orientation so as to obtain the diffraction peaks of all crystal planes. Refinements gave low *R*-factors (Table S1, Figure S2), and coordinates of atoms and main bond lengths are listed in Tables S2−S5. Smaller cell volumes of Mn^{2+}-doped BA_2PbX_4 (X = Cl, I) in comparison with cell volumes of hosts are usually in a good agreement with smaller ion radius of Mn^{2+} (0.67−0.83 Å, CN = 6) than that of Pb^{2+} (1.19 Å, CN = 6), however, cell parameters, *a* and *b* of Mn^{2+}-doped BA_2PbBr_4 increases and *c* value decreases leading to the nearly unchanged cell volume (Table S1). As shown in Figure 2a, the BA_2PbX_4 (X = Cl, Br, I) compounds prefer to grow along the ⟨001⟩ direction, and the alternating stacking of

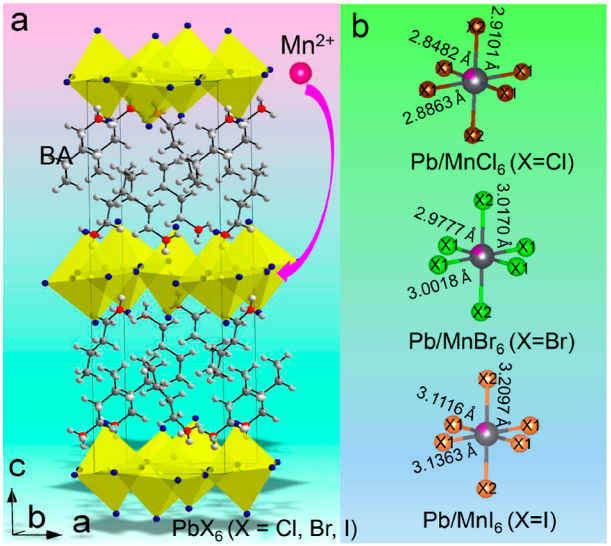

Figure 2. (a) Crystal structure of 2D perovskite BA_2PbX_4 (X = Cl, Br, I) viewed along the ⟨001⟩ direction. (b) Local structures of Pb/MnX_6 (X = Cl, Br, I) with different bond lengths and two equivalent positions X1 and X2 of the halogen atoms.

organic chain molecules and inorganic PbX_6 polyhedra, which are linked together by hydrogen bonds, induces the formation of a 2D layered perovskite structure.[10,29] Figure 2b highlights the coordination environment of the Pb/MnX_6 polyhedra with different bond lengths. The average bond lengths of Pb/Mn−X (Cl, Br, I) increase with the gradual substitution of I by Br or Br by Cl, implying that the crystal field intensity of luminescence center Mn^{2+} is adjustable through halogen exchange. The layered structure is also related to the morphological features of BA_2PbX_4 (X = Cl, Br, I), and the scanning electron microscopy (SEM) images in Figure S3 demonstrate the layered structure-like particle shape. Energy-dispersive X-ray spectroscopy (EDS) was used to confirm the elemental composition and uniformity of BA_2PbX_4 (X = Cl, Br, I) (see details in the Supporting Information, Figure S3).

It is well-known that halogen exchange affects the local environment of the luminescence center and thus is anticipated to realize the regulation of Mn emission. Therefore, a series of metal halides with different halogen ratios are synthesized. Figure 3a gives the XRD patterns of the 2D BA_2PbX_4 (X = Cl, Br, I) samples with different halogen contents, and the diffraction peaks (00*L*) possess preferred orientation, which further clarifies the feature of the layered structure. The obvious shift of diffraction peak positions also fully demonstrates successful halogen exchange. Meanwhile, diffuse reflectance spectra of these BA_2PbX_4 (X = Cl, Br, I) samples were measured (Figure 3b). Interestingly, the band gaps gradually decrease as Cl is substituted by Br and further by I. Because the band structures of the hosts have a great influence on the luminescence of dopants, it is possible for us to tune the Mn^{2+} emission by simple halogen exchange. On the basis of that, the luminescent properties of Mn^{2+}-doped BA_2PbX_4 were investigated in detail, as discussed below.

Figure 3c first demonstrates the intrinsic emissions of 2D BA_2PbX_4 (X = Cl, Br, I) hosts with different halogen contents. The band-edge emission of free excitons (FEs) is red-shifted when Cl is substituted by Br and I, which is consistent with the variation of the band gaps. For the compounds with halogen hybridizations, not only the band-edge emission of FEs but

DOI: 10.1021/acs.jpclett.9b01996
J. Phys. Chem. Lett. 2019, 10, 4706−4712

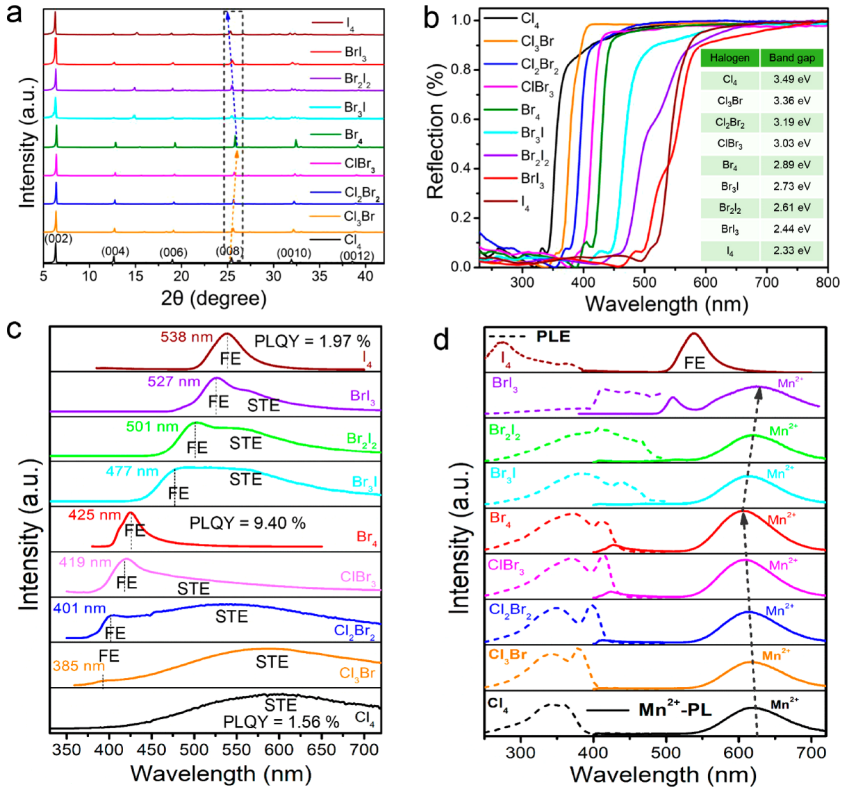

Figure 3. (a) Powder XRD patterns with different halogen contents of BA_2PbX_4 (X = Cl, Br, I) compounds and attribution of diffraction peaks on the (00*L*) crystal plane. (b) UV−vis diffuse reflectance spectra with different halogen contents of BA_2PbX_4 and corresponding band gaps calculated from the Tauc plot in the inset. (c) Normalized emission spectra of BA_2PbX_4 (X = Cl, Br, I) with different halogen contents. The dotted lines indicate the emission peak of FE, while the sign of STE stands for the emission of STE. (d) Normalized excitation and emission spectra of Mn^{2+}-doped samples $BA_2Pb_{0.8}Mn_{0.2}X_4$ with different halogen contents.

Table 1. Formation Energies of V_X at Different Positions (X1, X2) and Mn^{2+} in the BA_2PbX_4 (X = Cl, Br, I) Systems with V_{X2}[a]

Formation Energy (eV)					
BA_2PbCl_4		BA_2PbBr_4		BA_2PbI_4	
V_{Cl1}	V_{Cl2}	V_{Br1}	V_{Br2}	V_{I1}	V_{I2}
1.755	1.377	1.842	1.513	1.499	1.322
Mn(1)	Mn(2)	Mn(1)	Mn(2)	Mn(1)	Mn(2)
0.278	0.375	0.374	0.395	0.455	0.598

[a]Mn (1) and Mn (2) represent the doped Mn near and far from V_{X2}, respectively.

also the broad emissions of self-trapping excitons (STEs) with larger Stokes shifts caused by structural distortion can be observed.[30,31] However, the broad emission of STEs can only be detected in the host of Cl_4, unlike the band-edge emission of FEs exhibited in hosts of Br_4 and I_4. Furthermore, the luminescence intensities of BA_2PbCl_4 and BA_2PbI_4 systems are significantly lower than that of BA_2PbBr_4, and their corresponding photoluminescence quantum yields are 1.56, 1.97, and 9.4%, respectively. The dominant emissions of STEs in BA_2PbCl_4 and I-containing hybrid systems strongly imply the existence of defects. In BA_2PbX_4, the most abundant defects are well-verified to be halogen vacancies. Thus, we suppose that the Cl and I vacancy defects are more prone to be formed than Br vacancy defects, which decreases the luminescent efficiencies of the BA_2PbX_4 (X = Cl and I) due to the enhancement of nonradiative transition probability. To further clarify the existence of Cl and I vacancies, we performed DFT calculations to obtain the formation energies of V_X at different positions (X1, X2) in the BA_2PbX_4 (X = Cl, Br, I) systems. As shown in Figure 2b, the Pb atom is located in the center of the octahedron, and all positions are equivalent. Halogens have two equivalent positions, X1 and X2. Therefore, two kinds of vacancy defects, V_{X1} and V_{X2} (X = Cl, Br, I), were constructed, in which V_{X1} represents vacancies at the X1 position (X1−Pb−X1) and V_{X2} represents vacancies at the X2 position (−Pb−X2−Pb−) in the octahedral PbX_6. Considering the relative positions of Mn^{2+} impurities and halogen vacancies, Mn^{2+} doping is carried out at two locations. One is close to the halogen vacancies, and another is far from the halogen vacancies. It is well-known that formation energies can be used to judge the difficulty level of forming defects, including vacancy and impurity defects, and also to evaluate the stability of the system after forming defects. The formation energy of V_X is given by formula 1 as[32,33]

$$E_{f1} = E(V_X) - E(\text{pure}) + u_X(X = \text{Cl, Br, I}) \quad (1)$$

where E(X vacancy) is the total energy of the system that contains vacancy defects. E(pure) is the total energy of the intrinsic system, and u_X(X = Cl, Br, I) represents chemical

DOI: 10.1021/acs.jpclett.9b01996
J. Phys. Chem. Lett. 2019, 10, 4706−4712

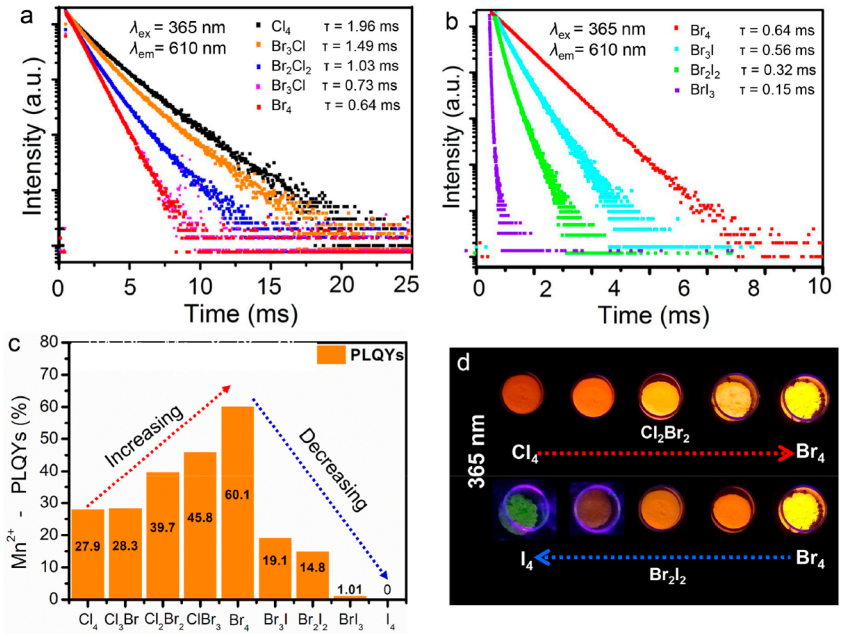

Figure 4. Decay curves of (a) $BA_2Pb_{0.8}Mn_{0.2}X_4$ (X = Cl, Br) and (d) $BA_2Pb_{0.8}Mn_{0.2}X_4$ (X = Br, I) of emission at 610 nm under 365 nm excitation. The inset in (a) gives the lifetimes in the range of 0.64−1.96 ms, and the inset in (b) shows the lifetimes in the range of 0.15−0.64 ms. (c) PPLQYs of $BA_2Pb_{0.8}Mn_{0.2}X_4$ (X = Cl, Br, I) under 365 nm excitation. $BA_2Pb_{0.8}Mn_{0.2}Br_4$ exhibits the highest PLQY of 60.1%. (d) Photographs of $BA_2Pb_{0.8}Mn_{0.2}X_4$ (X = Cl, Br, I) under 365 nm UV lamp, demonstrating different emission colors.

potentials of each atom of halogen group elements in the ground state.

As shown in Table 1, the formation energies of Br vacancies are higher than those of Cl and I (1.842 > 1.755 > 1.499; 1.513 > 1.377 > 1.322) in the three systems, indicating that the Br vacancy defects are relatively difficult to form, which is consistent with the observed luminescence in Figure 3c. Besides, the halogen vacancies at the V_{X2} position are more likely to form in the process of synthesis due to the lower formation energy of V_{X2} than that of V_{X1}. Then, the formation potential of Mn^{2+} doping was calculated by the following formula considering the existence of V_{X2}[32,33]

$$E_{f1} = E(\mathrm{Mn{-}V_{X2}}) - E(\mathrm{V_{X2}}) + u_{Pb} - u_{Mn} \quad (2)$$

where $E(\mathrm{Mn{-}V_{X2}})$ is the total energy of the system that contains both vacancy and dopant defects. $E(\mathrm{V_{X2}})$ is the total energy of the system containing V_{X2} defects, and u_{Pb} and u_{Mn} represent the chemical potentials of Pb and Mn in the ground state, respectively. The results (Table 1) show that Mn ions are more easily doped near V_{X2}, and thus, the following calculation will be based on this model.

As results of structural refinements in Figure S2, the Mn^{2+} occupies the position of Pb^{2+} with six-coordination. The normalized excitation and emission spectra of $BA_2Pb_{0.8}Mn_{0.2}X_4$ with different halogen contents are shown in Figure 3d. Under ultraviolet (UV) light excitation at 365 nm, the Mn^{2+}-doped samples exhibit broad bands consisting of a dominant peak at ~600 nm, arising from the $^4T_1{-}^6A_1$ transition of Mn^{2+}, and the typical narrow band emissions of the hosts. However, the broad-band emission of Mn^{2+} can hardly be observed in BA_2PbI_4, but only the narrow-band emission peaks at ~538 nm for FEs. The emission position of Mn^{2+} shifts slightly due to the change of the crystal field environment with the exchange of halogen ions. It is well-known that the luminescence of Mn^{2+} originates from the efficient energy transfer from excitons to Mn^{2+} ions, similar to the case of Mn^{2+}-doped 3D perovskites[34−36] and low-dimensional metal halides.[24,29] As confirmed above, the variety of halogens not only regulate the formation of vacancy defects but also adjust the electronic structure of hosts, which makes it possible to achieve the highly efficient luminescence of Mn^{2+} in metal halides by tuning the halogen content.

The decay curves of 610 nm emission are shown in Figure 4a,b, which are well fitted by a double-exponential decay process with $I = A_1 \exp(-t/\tau_1) + A_2 \exp(-t/\tau_2)$.[37] The average lifetimes, as shown in the insets, can be obtained by using the calculation formula $\tau = (A_1\tau_1^2 + A_2\tau_2^2)/(A_1\tau_1 + A_2\tau_2)$, ranging from 0.15 to 1.96 ms, which further proves that the broad-band emission can be attributed to the $^4T_1{-}^6A_1$ transition of Mn^{2+}. The lifetimes of Mn^{2+} decrease gradually as the Cl atoms are substituted by Br and I. It is noteworthy that the decay curve of Mn^{2+} in BA_2PbBr_4 tends to become a single-exponential function, which can infer that there are fewer defects in this system to hinder the radiation transition of Mn^{2+}, which is consistent with the above result on the calculated formation energies of V_X. Thus, highly efficient Mn^{2+} emission is obtained in BA_2PbBr_4, with the highest and record photoluminescence quantum yields (PLQY of 60.1%) in the 2D systems. As shown in Figure 4c, PLQYs of $BA_2Pb_{0.8}Mn_{0.2}X_4$ (X = Cl, Br, I) under 365 nm excitation show a trend of increasing first and then decreasing when the Cl atoms are substituted by Br and I. Moreover, the variation of emission intensity of Mn^{2+} can also be visualized from the photographs under a 365 nm UV lamp (Figure 4d), which clearly show the bright yellow luminescence of Mn^{2+} in BA_2PbBr_4.

In addition, the role of halogens on electronic structure is further discussed by using DFT calculations. As shown in Figure S4, the band gaps of BA_2PbX_4 (X = Cl, Br, I) without considering defects of vacancies and impurities are 3.13, 2.55, and 2.22 eV, respectively, which is basically in agreement with the experimental results (Figure 3b). It can be shown that the valence band maximum (VBM) of the intrinsic system consists

DOI: 10.1021/acs.jpclett.9b01996
J. Phys. Chem. Lett. 2019, 10, 4706−4712

of the p orbitals of halogens and a few 6p orbitals of Pb, and the conduction band minimum (CBM) consists mainly of the Pb-6p orbitals and minorly of halogen p orbitals. According to Figure S5, the energy levels of vacancy defects appear just below the CBM in all three systems, and the halogens p orbitals and the Pb-6p orbitals are hybridized at the CBM. When Mn^{2+} is doped in the systems containing halogen vacancies, the charge density differences of the systems (Figure 5a–c) reveal that when Mn^{2+} enters the center of the crystal

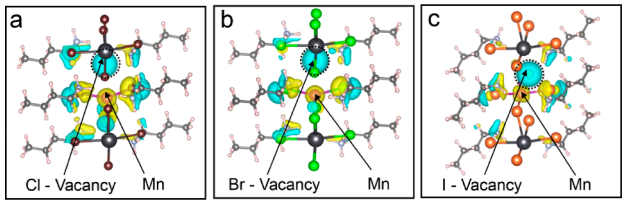

Figure 5. Charge density difference of systems with a halogen vacancy (V_{X2}) and impurity Mn^{2+}: (a) BA_2PbCl_4; (b) BA_2PbBr_4; (c) BA_2PbI_4. The yellow (light blue) region indicates the charge accumulation (depletion), and the isosurface level is 0.05 electron/Bohr^3.

lattice to replace Pb^{2+}, the extra electrons caused by vacancies of halogen are captured and the Pb/Mn–X bond is formed by charge transfer of the dopant with surrounding halogens, which makes the doped Mn^{2+} tend to exchange energy with the host.

Notably, the hybrid coupling of the Mn-3d orbitals with the Pb-6p orbitals and halogen p orbitals can be seen from the band structure. An enlarged view of the CBM and DOS of the systems with halogen vacancy (V_{X2}) and impurity Mn^{2+}, shown in Figure 6, further confirms that Mn^{2+} contributes to the composition of conduction bands in the systems. This meets the basic requirement of efficient energy transfer from the host to the dopant. Moreover, Mn^{2+} produces obvious impurity levels in the forbidden bands of the hosts. These impurity levels are located below the CBM and near the VBM in BA_2PbCl_4, while they distribute dispersedly within the forbidden band of BA_2PbI_4. Notably, the impurity levels only appear above the valence band in BA_2PbBr_4.

These great differences that Mn^{2+} ions bring to the band structure of the three systems cause the different energy transfer processes, as shown in Figure 7. In process (1), the excited electrons jump from the valence band to the conduction band, accompanied by the emergence of holes in the valence band. For the system of BA_2PbCl_4 (Figure 7a), the excited electrons can relax to the Mn-3d level below the CBM, causing some energy loss, as in process (2). The free electrons at the Mn-3d level can be captured in traps produced by the thermally emptied V_{Cl2} (process 3), while others can directly recombine with holes at the Mn-3d level near the VBM (process 4) to realize $^4T_1$–$^6A_1$ transition of Mn^{2+}. Although the captured electrons at the V_{Cl2} level can be re-released to the conduction band (process 5) due to thermal excitation, it is inevitable that some electrons will not be able to transit back to the Mn-3d level due to energy transfer or thermal motion, thus reducing the luminescence efficiency.

For the BA_2PbBr_4 system (Figure 7b), the Mn-3d level and the Pb-6p level of the host are hybridized at the CBM, and the Mn-3d level at the CBM can easily obtain a large number of excited electrons. Therefore, free electrons can transit directly from the excited state of the Mn-3d level to the ground state of the Mn-3d level, so as to achieve efficient luminesce of Mn^{2+}. Moreover, the energy loss caused by the trap level can be suppressed due to the low concentration of Br vacancy. High-efficiency Mn^{2+} emission reveals that $BA_2Pb_{0.8}Mn_{0.2}Br_4$ has promising potential for solid-state lighting. However, for the BA_2PbI_4 system with V_{I2} (Figure 7c), the Mn-3d levels are distributed dispersedly in both conduction and forbidden bands. There are a large number of impurity levels in the forbidden band. When the free electrons relax from the CBM to the Mn-3d levels, the energy can be easily released by lattice vibration because of the small energy difference of the local

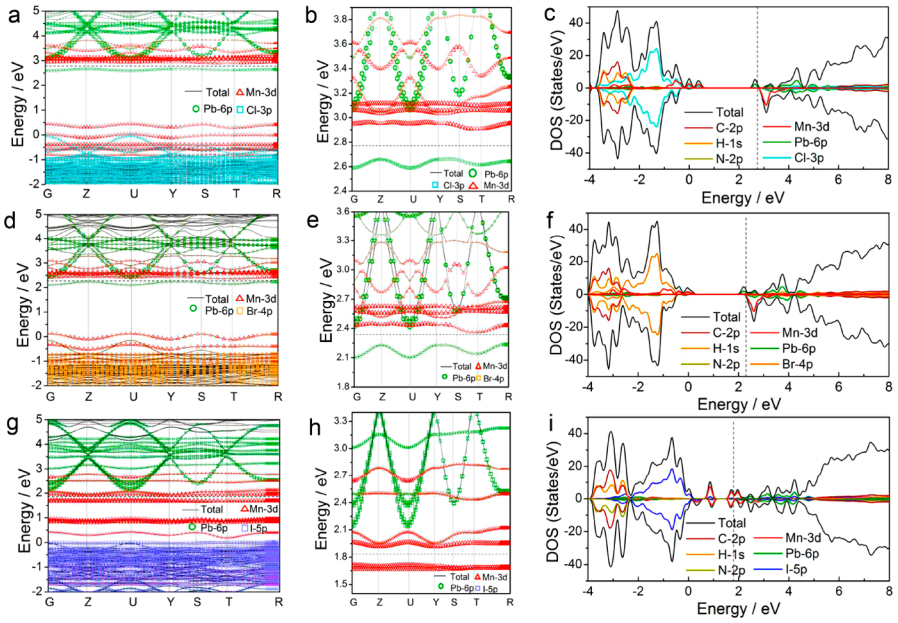

Figure 6. Band structure (a,d,g), enlarged view of the CBM (b,e,h), and DOS (c,f,i) of the systems with a halogen vacancy (V_{X2}) and impurity Mn^{2+}: (a–c) BA_2PbCl_4; (d–f) BA_2PbBr_4; (g–i) BA_2PbI_4. The symbol size in the lines of the band structure represents the characteristic weight of Mn-d, Pb-p, and X-p (X = Cl, Br and I) orbitals, respectively.

DOI: 10.1021/acs.jpclett.9b01996
J. Phys. Chem. Lett. 2019, 10, 4706–4712

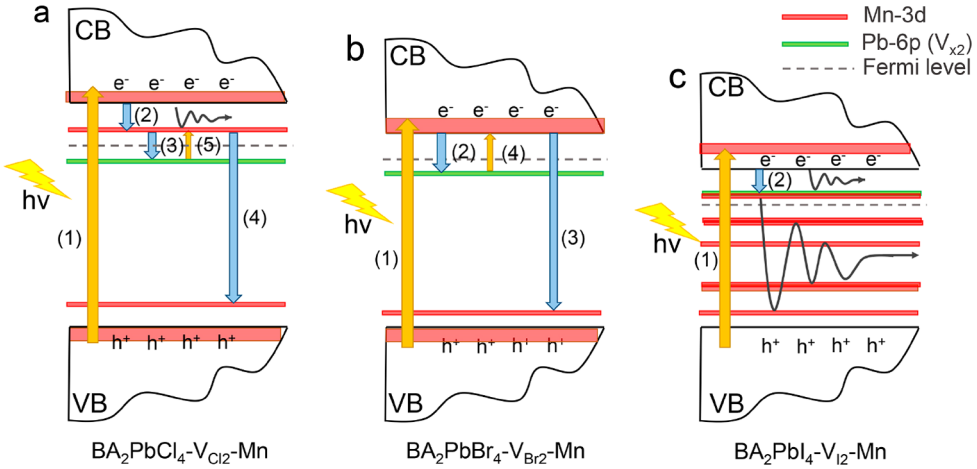

Figure 7. Proposed schematic models on the exciton−dopant exchange coupling with the halogen vacancy (V_{X2}) and impurity Mn^{2+} in different systems: (a) BA_2PbCl_4; (b) BA_2PbBr_4; (c) BA_2PbI_4.

energy levels, thus causing numerous nonradiative transitions. Therefore, the Mn^{2+} emission is undetectable.

In summary, we investigated the layered halide perovskites BA_2PbX_4 to highlight the role of the halogens on the Mn^{2+} emission, and tunable emission could be achieved by designing appropriate halogen contents. The nature of the halogen has been verified to be a critical factor parameter to tune the V_{X2} defects and the electronic structures of the BA_2PbX_4 hosts, which will greatly influence the properties of the dopants. BA_2PbBr_4 has low Br vacancy concentration and coupled orbitals of Mn-3d and Pb-6p, which enable efficient energy transfer between the host and Mn ions, leading to highly efficient Mn^{2+} luminescence. The tuning of halogen contents is of high importance for optimizing luminescent properties, and our realizable cases could provide a new understanding of the exciton−dopant exchange mechanism in metal halides and inspire the search of high-efficiency dopant luminescence by fine tailoring of the host property.

■ ASSOCIATED CONTENT

Supporting Information

The Supporting Information is available free of charge on the ACS Publications website at DOI: 10.1021/acs.jpclett.9b01996.

Experimental details, Figures S1−S5 showing synthesis illustrations, Rietveld refinement patterns, morphology pictures and analysis results, and band structures and densities of states of the systems, and Tables S1−S5, providing main parameters of processing and refinement, fractional atomic coordinates and isotropic displacement parameters, and main geometric parameters (PDF)

■ AUTHOR INFORMATION

Corresponding Authors

*E-mail: zjy@buaa.edu.cn.
*E-mail: xiazg@scut.edu.cn.

ORCID

Junying Zhang: 0000-0002-4860-8774
Zhiguo Xia: 0000-0002-9670-3223

Author Contributions

#G.Z. and X.J. contributed equally to this work.

Notes

The authors declare no competing financial interest.

■ ACKNOWLEDGMENTS

This work is supported by the National Natural Science Foundation of China (No. 51722202 and 51572023), the Natural Science Foundations of Beijing (2172036), the Fundamental Research Funds for the Central Universities (FRF-TP-18-002C1), and the Guangdong Provincial Science & Technology Project (No. 2018A050506004).

■ REFERENCES

(1) Fu, W.; Wang, J.; Zuo, L.; Gao, K.; Liu, F.; Ginger, D. S.; Jen, A. K. Y. Two-Dimensional Perovskite Solar Cells with 14.1% Power Conversion Efficiency and 0.68% External Radiative Efficiency. *ACS Energy Lett.* **2018**, *3*, 2086−2093.

(2) Yusoff, A. R. b. M.; Nazeeruddin, M. K. Low-Dimensional Perovskites: from Synthesis to Stability in Perovskite Solar Cells. *Adv. Energy Mater.* **2018**, *8*, 1702073.

(3) Tian, Y.; Zhou, C. K.; Worku, M.; Wang, X.; Ling, Y. C.; Gao, H. W.; Zhou, Y.; Miao, Y.; Guan, J. J.; Ma, B. W. Highly Efficient Spectrally Stable Red Perovskite Light-Emitting Diodes. *Adv. Mater.* **2018**, *30*, 1707093.

(4) Cao, D. H.; Stoumpos, C. C.; Farha, O. K.; Hupp, J. T.; Kanatzidis, M. G. 2D Homologous Perovskites as Light-Absorbing Materials for Solar Cell Applications. *J. Am. Chem. Soc.* **2015**, *137*, 7843−7850.

(5) Chen, P.; Bai, Y.; Lyu, M. Q.; Yun, J. H.; Hao, M. M.; Wang, L. Z. Progress and Perspective in Low-Dimensional Metal Halide Perovskites for Optoelectronic Applications. *Sol. RRL.* **2018**, *2*, 1700186.

(6) Liu, Z.; Li, C.; Shang, Q. Y.; Zhao, L. Y.; Zhong, Y. G.; Gao, Y.; Du, W. N.; Mi, Y.; Chen, J.; Zhang, S.; Liu, X. F.; Fu, Y. S.; Zhang, Q. Research Progress of Low-Dimensional Metal Halide Perovskites for Lasing Applications. *Chin. Phys. B* **2018**, *27*, 114209.

(7) Wei, Y.; Cheng, Z.; Lin, J. An Overview on Enhancing the Stability of Lead Halide Perovskite Quantum Dots and Their Applications in Phosphor-Converted LEDs. *Chem. Soc. Rev.* **2019**, *48*, 310−350.

(8) Ding, J.; Cheng, X.; Jing, L.; Zhou, T.; Zhao, Y.; Du, S. Polarization-Dependent Optoelectronic Performances in Hybrid Halide Perovskite $MAPbX_3$ (X = Br, Cl) Single-Crystal Photodetectors. *ACS Appl. Mater. Interfaces* **2018**, *10*, 845−850.

(9) Dou, L. T.; Wong, A. B.; Yu, Y.; Lai, M. L.; Kornienko, N.; Eaton, S. W.; Fu, A.; Bischak, C. G.; Ma, J.; Ding, T.; Ginsberg, N. S.; Wang, L. W.; Alivisatos, A. P.; Yang, P. D. Tomically Thin Two-

DOI: 10.1021/acs.jpclett.9b01996
J. Phys. Chem. Lett. 2019, 10, 4706−4712

Dimensional Organic-Inorganic Hybrid Perovskites. *Science* **2015**, *349*, 1518−1521.
(10) Dutta, S. K.; Dutta, A.; Das Adhikari, S.; Pradhan, N. Doping Mn^{2+} in Single-Crystalline Layered Perovskite Microcrystals. *ACS Energy Lett.* **2019**, *4*, 343−351.
(11) Swarnkar, A.; Ravi, V. K.; Nag, A. Beyond Colloidal Cesium Lead Halide Perovskite Nanocrystals: Analogous Metal Halides and Doping. *ACS Energy Lett.* **2017**, *2*, 1089−1098.
(12) Begum, R.; Parida, M. R.; Abdelhady, A. L.; Murali, B.; Alyami, N. M.; Ahmed, G. H.; Hedhili, M. N.; Bakr, O. M.; Mohammed, O. F. Engineering Interfacial Charge Transfer in $CsPbBr_3$ Perovskite Nanocrystals by Heterovalent Doping. *J. Am. Chem. Soc.* **2017**, *139*, 731−737.
(13) van der Stam, W.; Geuchies, J. J.; Altantzis, T.; van den Bos, K. H.; Meeldijk, J. D.; Van Aert, S.; Bals, S.; Vanmaekelbergh, D.; de Mello Donega, C. Highly Emissive Divalent-Ion-Doped Colloidal $CsPb_{1-x}M_xBr_3$ Perovskite Nanocrystals through Cation Exchange. *J. Am. Chem. Soc.* **2017**, *139*, 4087−4097.
(14) Gautier, R.; Massuyeau, F.; Galnon, G.; Paris, M. Lead Halide Post-Perovskite-Type Chains for High-Efficiency White-Light Emission. *Adv. Mater.* **2019**, *31*, 1807383.
(15) Hu, H. W.; Meier, F.; Zhao, D. M.; Abe, Y.; Gao, Y.; Chen, B. B.; Salim, T.; Chia, E. E. M.; Qiao, X. F.; Deibel, C.; Lam, Y. M. Efficient Room-Temperature Phosphorescence from Organic-Inorganic Hybrid Perovskites by Molecular Engineering. *Adv. Mater.* **2018**, *30*, 1707621.
(16) Guria, A. K.; Dutta, S. K.; Das Adhikari, S.; Pradhan, N. Doping Mn^{2+} in Lead Halide Perovskite Nanocrystals: Successes and Challenges. *ACS Energy Lett.* **2017**, *2*, 1014−1021.
(17) Zhou, J.; Rong, X.; Zhang, P.; Molokeev, M. S.; Wei, P.; Liu, Q.; Zhang, X.; Xia, Z. Manipulation of Bi^{3+}/In^{3+} Transmutation and Mn^{2+}-Doping Effect on the Structure and Optical Properties of Double Perovskite $Cs_2NaBi_{1-x}In_xCl_6$. *Adv. Opt. Mater.* **2019**, *7*, 1801435.
(18) Karmakar, A.; Dodd, M. S.; Agnihotri, S.; Ravera, E.; Michaelis, V. K. Cu(II)-Doped $Cs_2SbAgCl_6$ Double Perovskite: A Lead-Free, Low-Bandgap Material. *Chem. Mater.* **2018**, *30*, 8280−8290.
(19) Majher, J. D.; Gray, M. B.; Strom, T. A.; Woodward, P. M. $Cs_2NaBiCl_6$:Mn^{2+}-A New Orange-Red Halide Double Perovskite Phosphor. *Chem. Mater.* **2019**, *31*, 1738−1744.
(20) Zhou, Y.; Chen, J.; Bakr, O. M.; Sun, H. T. Metal-Doped Lead Halide Perovskites: Synthesis, Properties, and Optoelectronic Applications. *Chem. Mater.* **2018**, *30*, 6589−6613.
(21) Cortecchia, D.; Dewi, H. A.; Yin, J.; Bruno, A.; Chen, S.; Baikie, T.; Boix, P. P.; Gratzel, M.; Mhaisalkar, S.; Soci, C.; Mathews, N. Lead-Free $MA_2CuCl_xBr_{4-x}$ Hybrid Perovskites. *Inorg. Chem.* **2016**, *55*, 1044−1052.
(22) Cai, T.; Yang, H.; Hills-Kimball, K.; Song, J. P.; Zhu, H.; Hofman, E.; Zheng, W.; Rubenstein, B. M.; Chen, O. Synthesis of All-Inorganic Cd-Doped $CsPbCl_3$ Perovskite Nanocrystals with Dual-Wavelength Emission. *J. Phys. Chem. Lett.* **2018**, *9*, 7079−7084.
(23) Yangui, A.; Pillet, S.; Bendeif, E.; Lusson, A.; Triki, S.; Abid, Y.; Boukheddaden, K. Broadband Emission in a New Two-Dimensional Cd-Based Hybrid Perovskite. *ACS Photonics* **2018**, *5*, 1599−1611.
(24) Zhou, C. K.; Tian, Y.; Khabou, O.; Worku, M.; Zhou, Y.; Hurley, J.; Lin, H. R.; Ma, B. W. Manganese-Doped One-Dimensional Organic Lead Bromide Perovskites with Bright White Emissions. *ACS Appl. Mater. Interfaces* **2017**, *9*, 40446−40451.
(25) Das Adhikari, S.; Dutta, A.; Dutta, S. K.; Pradhan, N. Layered Perovskites $L_2(Pb_{1-x}Mn_x)Cl_4$ to Mn-doped $CsPbCl_3$ Perovskite Platelets. *ACS Energy Lett.* **2018**, *3*, 1247−1253.
(26) Bakthavatsalam, R.; Biswas, A.; Chakali, M.; Bangal, P. R.; Kore, B. P.; Kundu, J. Temperature-Dependent Photoluminescence and Energy-Transfer Dynamics in Mn^{2+}-Doped $(C_4H_9NH_3)_2PbBr_4$ Two-Dimensional (2D) Layered Perovskite. *J. Phys. Chem. C* **2019**, *123*, 4739−4748.
(27) Luo, B. B.; Li, F.; Xu, K.; Guo, Y.; Liu, Y.; Xia, Z. G.; Zhang, J. Z. B-Site Doped Lead Halide Perovskites: Synthesis, Band Engineering, Photophysics, and Light Emission Applications. *J. Mater. Chem. C* **2019**, *7*, 2781−2808.
(28) Tan, Z. F.; Li, J. H.; Zhang, C.; Li, Z.; Hu, Q. S.; Xiao, Z. W.; Kamiya, T.; Hosono, H.; Niu, G. D.; Lifshitz, E.; Cheng, Y. B.; Tang, J. Highly Efficient Blue-Emitting Bi-Doped Cs_2SnCl_6 Perovskite Variant: Photoluminescence Induced by Impurity Doping. *Adv. Funct. Mater.* **2018**, *28*, 1801131.
(29) Biswas, A.; Bakthavatsalam, R.; Kundu, J. Efficient Exciton to Dopant Energy Transfer in Mn^{2+}-Doped $(C_4H_9NH_3)_2PbBr_4$ Two-Dimensional (2D) Layered Perovskites. *Chem. Mater.* **2017**, *29*, 7816−7825.
(30) Cai, P.; Wang, X.; Seo, H. J.; Yan, X. Bluish-White-Light-Emitting Diodes Based on Two-Dimensional Lead Halide Perovskite $(C_6H_5C_2H_4NH_3)_2PbCl_2Br_2$. *Appl. Phys. Lett.* **2018**, *112*, 153901.
(31) Smith, M. D.; Karunadasa, H. I. White-Light Emission from Layered Halide Perovskites. *Acc. Chem. Res.* **2018**, *51*, 619−627.
(32) Kang, J.; Wang, L. W. High Defect Tolerance in Lead Halide Perovskite $CsPbBr_3$. *J. Phys. Chem. Lett.* **2017**, *8*, 489−493.
(33) Guo, S. Q.; Wang, Y. Y.; Wang, C.; Tang, Z. L.; Zhang, J. Y. Large Spin-Orbit Splitting in the Conduction Band of Halogen (F, Cl, Br, and I) Doped Monolayer WS_2 with Spin-Orbit Coupling. *Phys. Rev. B: Condens. Matter Mater. Phys.* **2017**, *96*, 245305.
(34) Yin, J.; Ahmed, G. H.; Bakr, O. M.; Bredas, J. L.; Mohammed, O. F. Unlocking the Effect of Trivalent Metal Doping in All-Inorganic $CsPbBr_3$ Perovskite. *ACS Energy Lett.* **2019**, *4*, 789−795.
(35) Liu, W. Y.; Lin, Q. L.; Li, H. B.; Wu, K. F.; Robel, I.; Pietryga, J. M.; Klimov, V. I. Mn^{2+}-Doped Lead Halide Perovskite Nanocrystals with Dual-Color Emission Controlled by Halide Content. *J. Am. Chem. Soc.* **2016**, *138*, 14954−14961.
(36) Li, F.; Xia, Z. G.; Pan, C. F.; Gong, Y.; Gu, L.; Liu, Q. L.; Zhang, J. Z. High Br^- Content $CsPb(ClyBr_{1-y})_3$ Perovskite Nanocrystals with Strong Mn^{2+} Emission through Diverse Cation/Anion Exchange Engineering. *ACS Appl. Mater. Interfaces* **2018**, *10*, 11739−11746.
(37) Huang, C. H.; Chen, T. M.; Liu, W. R.; Chiu, Y. C.; Yeh, Y. T.; Jang, S. M. A Single-Phased Emission-Tunable Phosphor $Ca_9Y(PO_4)_7$:Eu^{2+}, Mn^{2+} with Efficient Energy Transfer for White-Light-Emitting Diodes. *ACS Appl. Mater. Interfaces* **2010**, *2*, 259−264.

DOI: 10.1021/acs.jpclett.9b01996
J. Phys. Chem. Lett. 2019, 10, 4706−4712